EFFECT OF ELEVATED TEMPERATURE ON CERAMIC ULTRAFILTRATION OF COLLOIDAL SUSPENSIONS

A Master's Thesis
Presented to
The Academic Faculty

by

Tyler Thorleif Cromey

In Partial Fulfillment
of the Requirements for the Degree
Master of Science in the
School of Civil and Environmental Engineering

Georgia Institute of Technology
May 2014

EFFECT OF ELEVATED TEMPERATURE ON CERAMIC ULTRAFILTRATION OF COLLOIDAL SUSPENSIONS

Approved by:

Dr. Jaehong Kim, Advisor
School of Civil and Environmental Engineering
Georgia Institute of Technology

Dr. Ching-Hua Huang
School of Civil and Environmental Engineering
Georgia Institute of Technology

Dr. John Koon, P.E.
School of Civil and Environmental Engineering
Georgia Institute of Technology

Date Approved: April 4, 2014

ACKNOWLEDGEMENTS

I wish to express my deepest thanks to my advisor Dr. Jaehong Kim and committee members, Dr. Ching-Hua Huang and Dr. John Koon, P.E. for their wisdom and support throughout my graduate studies at the Georgia Institute of Technology. I especially would like to thank Dr. Kim for his support, supervision, encouragement, and most importantly friendship. Without his guidance none of this would have been possible and I am truly thankful for what he has done for me.

I would also like to express my gratitude to Chuck Huling and the Georgia Power Company for their generous support of my research. This work was only possible because of their generosity and dedication to higher education.

Thank you to all of Dr. Kim's fellow group members and colleagues for your advice and the good times we have had together. Particularly my thanks go to Seungjin Lee who was a crucial resource through each stage of my research.

I would like to thank the department faculty and staff for their helpfulness and guidance during my time spent here at Georgia Tech. A special thanks to Jenny Eaton for always ensuring that I had everything I needed to be successful.

Finally, I want to thank my friends and family for being there for me through all of these long years of schooling. They are the ones who have kept me going and urged me to pursue my dreams. And of course I want to thank my loving and caring wife Lydia for making my life complete.

TABLE OF CONTENTS

LIST OF TABLES

LIST OF FIGURES

LIST OF SYMBOLS

a	adhesive distance between two spheres [m]
a_p	particle radius [m]
α	specific cake resistance [m/g]
d_p	particle diameter [m]
ΔP	applied transmembrane pressure [Pa]
δ_c	cake layer thickness [m]
ε	cake porosity
η	dynamic viscosity [Pa·s]
F_A	adhesive force [N]
F_D	drag force due to the cross-flow [N]
F_F	friction force [N]
F_L	lift force [N]
F_N	normal force [N]
F_P	drag force due to the permeate flux [N]
F_x	resultant force in the x-direction [N]
F_y	resultant force in the y-direction [N]
$\hbar\varpi$	Lifschitz-van der Waals constant [10^{-20} J]
J	permeate flux [m/s]
λ	concentration correction factor
M_c	number of particles accumulated in the cake layer per unit [#/m^2]
M_d	mass deposited per unit area on the membrane surface [g/m^2]
μ	coefficient of friction
φ_s	volume concentration

R^2	coefficient of determination
R_{cr}	chemically removable resistance [m^{-1}]
R_{if}	chemically irreversible resistance [m^{-1}]
R_m	membrane resistance [m^{-1}]
R_{pr}	physically removable resistance [m^{-1}]
R_t	total resistance [m^{-1}]
ρ	particle density [kg/m^3]
τ_w	shear stress [Pa]
v	undistributed velocity/cross-flow velocity [m/s]

LIST OF ABBREVIATIONS

FGD	flue gas desulfurization
LMH	a unit of flux, liter per square meter per hour [$l/m^2/h$]
TMP	transmembrane pressure

SUMMARY

The inherent thermal resistance of ceramic membranes allows for treatment of industrial waters at elevated temperatures. Traditionally, the high temperature of wastewater has been an issue compromising the integrity of polymeric membrane systems or requiring the temperature to be lowered for further treatment. In ceramic membrane systems, however, a decrease in viscosity with increasing temperature can be utilized as an advantage since the temperature increase is accompanied by a corresponding increase in the permeate flux. In this study, the fouling of ceramic ultrafiltration membranes by feed solutions containing colloidal silica was evaluated at temperatures seen in various industries between 25 – 90 °C. Ceramic membranes performed well at elevated temperatures up to 90 ºC with sustained mechanical and chemical integrity. Results showed net benefit of filtration at elevated temperatures on permeate flux in spite of increasing total fouling resistance with temperature. When the temperature increased from 25 to 90 °C, there was a 90% increase in steady-state permeate flux. The increase in permeate flux was primarily attributed to decreasing viscosity; however, the benefit was diminished during filtration of the colloidal silica due to fouling. The dominant resistance was physically removable fouling, which was easily removed and allowed for full flux recovery, while chemically removable and irreversible fouling were negligible at all temperatures. The observed increase in fouling with feed temperature was supported by force balance analyses. The cake layer mass and thickness increased by 71 and 51%, respectively, from 25 to 90 °C indicating that more intense fouling occurred at higher temperatures. This study provides a foundation from which further studies can be developed including pilot-scale testing, use of real wastewater, and the effects of operating conditions.

I. INTRODUCTION

1.1. Motivation for research

Many industries require the treatment of wastewater and the production of liquid products at high temperatures [1, 2]. Membrane filtration is frequently used in the treatment of various industrial feeds at high temperatures and is often preferred [3, 4]. In the food processing industry, membranes are used for the clarification of fruit juices which can be over 50 °C [3], and the sugar industry requires temperatures of 70 – 98 °C in order to prevent biological growth [1, 3]. Other examples include pulp and paper industry wastewaters with maximum temperatures between 60 – 70 °C [2], and textile industry wastewaters which can reach temperatures of 90 – 95 °C [4], but are treated by membranes at lower temperatures from 50 – 70 °C [5]. The wastewater from coal-fired power plants can also be as hot as 50 – 60 °C and needs to be treated at that temperature or cooled before treatment [6]. Tremendous filtration potential is lost by lowering the temperature of the wastewater due to the increased viscosity which leads to lower permeate flux [7-9]. Therefore, a membrane process capable of operating at elevated temperature without compromising integrity of the membranes and providing industrial processes with durability is desirable. Polymeric membranes have narrower operating ranges (i.e. temperatures up to 75 °C, pH 2 – 11, and pressure less than 7 bar) [10, 11], and are prone to degradation and loss of functionality at temperatures exceeding 75 °C [8, 12]. Ceramic membranes are fully capable of operating at temperatures up to 350 °C, any pH, and at pressures up to 15 bar due to the inherent thermal stability and robustness of the membrane [11].

There are many intrinsic benefits for filtration by treating wastewater at elevated temperatures. It is well known that as temperature increases, the viscosity of a solution decreases which leads to a higher permeate flux. Additionally, the diffusion coefficient is known to increase as temperature increases [13]. A greater diffusion coefficient means that particles will diffuse through the membrane at a faster rate. In a previous study on the filtration of polyethylene glycol, it was found that increasing filtration temperature led to lower initial fouling resistances [14]. Particle-particle interactions in a solution can become more beneficial at raised temperatures as well. The double layer thickness increases with temperature, which leads to greater stability of colloidal particles, and it has been shown that the filtration rate of colloidal particles increases with increasing stability [15, 16]. It is clear that operation at higher temperatures takes advantage of beneficial particle and solution conditions which leads to more desirable filtration conditions.

1.2. Ceramic membrane characteristics

Ceramic membranes are made from inorganic materials (e.g. oxides of Al, Si, Ti, or Zr) which provides them with greater chemical and thermal resistivity [17]. This permits more aggressive cleaning approaches which allow for increased recovery of membrane functionality, subsequently prolonging membrane life and decreasing downtime for maintenance and cleaning [18, 19]. The superior structural integrity of ceramic membranes decreases the likelihood of membrane failure and the need to replace broken membranes [20], and extends the expected service life to at least 20 years compared to 7 – 10 years for a polymeric membrane [10]. Ceramic membranes are also capable of operation in extreme environments with a wider

operational temperature, pH, and pressure range [10]. Furthermore, with recent advances in ceramic membrane manufacturing and subsequent decreasing costs, ceramic membranes are becoming a more viable option in industrial wastewater treatment [21].

1.3. Objective

The objective of this study was to evaluate the effect of elevated temperatures on the fouling behavior of ceramic membranes during the filtration of colloidal silica. There is very little information available in the literature on the effect of elevated operating temperatures on ceramic membrane filtration and subsequent fouling and this work aims to provide a comprehensive study over a wide range of temperatures which are seen in different industries. Colloidal silica was selected as a model foulant as it has been widely used in previous studies investigating membrane fouling [9, 22-24] and for the frequency of colloidal particles in industrial waters [23]. A bench-scale filtration system was employed in constant pressure cross-flow mode, which ensures higher flux, in comparison to dead-end mode, due to reduction in membrane fouling [25]. Hence, experiments were performed at temperatures between 25 – 90 °C to evaluate their effects on flux and membrane fouling. Flux data were used to analyze the fouling resistances by the resistance-in-series model, and characterization of the cake layer was achieved through analysis of cake layer properties, i.e. mass, porosity, and thickness.

II. Materials and Methods

2.1. Materials

2.1.1. Ceramic membranes

Disc-type ceramic membranes were supplied by Sterlitech Corp. (Kent, WA). The membranes are 2.5 mm thick and 90 mm in diameter with an effective filtration area of 56.3 cm^2 and a molecular weight cut-off of 50 kDa. The maximum operating temperature and pressure of the membranes is 350 °C and 4 bar, respectively, and the acceptable pH range is 0-14. Virgin membranes were initially chemically cleaned as suggested by the manufacturer to remove any residue from the manufacturing process and then washed in ultrapure water (resistivity >18.2 MΩ) to wet the membrane. Used and brand new membranes were chemically cleaned according to the following procedure: soaking in 0.1 N NaOH at 85 °C for 15 min, followed by neutralization by rinsing in ultrapure water, then soaking in 0.2 N phosphoric acid at 50 °C for 15 min, and finally neutralization again. Membranes were stored in ultrapure water in between uses.

2.1.2. Feed solutions

Feed solutions were prepared by diluting a 40 wt. % suspension of colloidal silica nanoparticles (Sigma-Aldrich, Ludox® AS-40, Milwaukee, WI) to 1.25 wt. % using ultrapure water to make a total feed volume of about 2 L. The pH was adjusted to 7.0 using HCl and NaOH. Particle diameter and zeta potential were measured using a Zetasizer Nano ZS (Malvern,

UK). The colloidal silica is monodisperse with a particle diameter of 34 ± 0.1 nm and a zeta potential of -40.7 ± 0.1 mV at 25 °C and pH 8.9.

A synthetic flue gas desulfurization (FGD) wastewater was developed and used in fouling experiments based off of the wastewater created in the studies by Nakajima et al. [26]. Fouling experiments using this wastewater were to be used as a determinant of the applicability of ceramic membrane treatment at elevated temperatures for FGD wastewater in coal-fired power plants. The particular experimental design used in this study, combined with the high salt and total suspended solids content of the synthetic wastewater, provided inconclusive results. This was due to the buildup of salts in the membrane module channel which was limited in size by the spacer designed to be used with the module. While this study focused primarily on colloidal silica, information pertaining to the synthetic FGD wastewater experiments can be found in Appendix B.

2.2. Filtration experiments

A stainless steel cross-flow membrane module (TAMI Industries, INSIDE DisRAM™, Montréal, Québec, Canada) housed the membrane during filtration. The system was maintained at a constant pressure of 1.0 ± 0.1 bar by adjusting a needle valve on the retentate line and the trans-membrane pressure (TMP) was monitored by a pressure transmitter (Omega, PX409-100GUSB, Stamford, CT). Cross-flow velocity was kept constant at 0.60 ± 0.03 m/s by a peristaltic pump, and the flow rate was monitored using a digital flowmeter (McMillan Co., 114 Flo-meter, Georgetown, TX). Feed temperature was maintained using a stirring hot plate

connected to a temperature probe with external temperature control (IKA Works Inc., L005457, Wilmington, NC). A schematic diagram of the experimental setup is shown in Fig. 1 and a photograph of the equipment is seen in Fig. 2. In order to prevent any temperature gradient from forming in the system, the membrane module was kept inside of a gravity convection oven set to the experimental temperature. A flow-through temperature sensor (Cole-Parmer, XS-00309-MX, Vernon Hills, IL) monitored temperature before the feed passed through the membrane module. Retentate flow was recycled back to the feed reservoir while permeate was collected on a digital balance (Mettler Toledo, PL3001-S, Columbus, OH) and the cumulative weight recorded via a computer communicating with the balance. The flux and cumulative volume were calculated using the mass recorded at specific time intervals. Permeate was frequently returned to the feed reservoir so that the system was run in complete recycle mode. Any water lost due to evaporation was replenished with ultrapure water. At the start of experiments, the system temperature was allowed to equilibrate by passing the feed through the module with the retentate line fully open and the permeate line closed. After the system reached equilibrium, the permeate line was opened and back pressure was applied on the retentate side to achieve the desired TMP. The final volume of filtration in all experiments was 422 mL or 75 L/m^2 which is the specific volume filtered per unit area of membrane. Solute rejection was measured by comparing the absorbance of samples of the feed and permeate at 250 nm using a UV-Vis spectrophotometer (Agilent 8453, Santa Clara, CA).

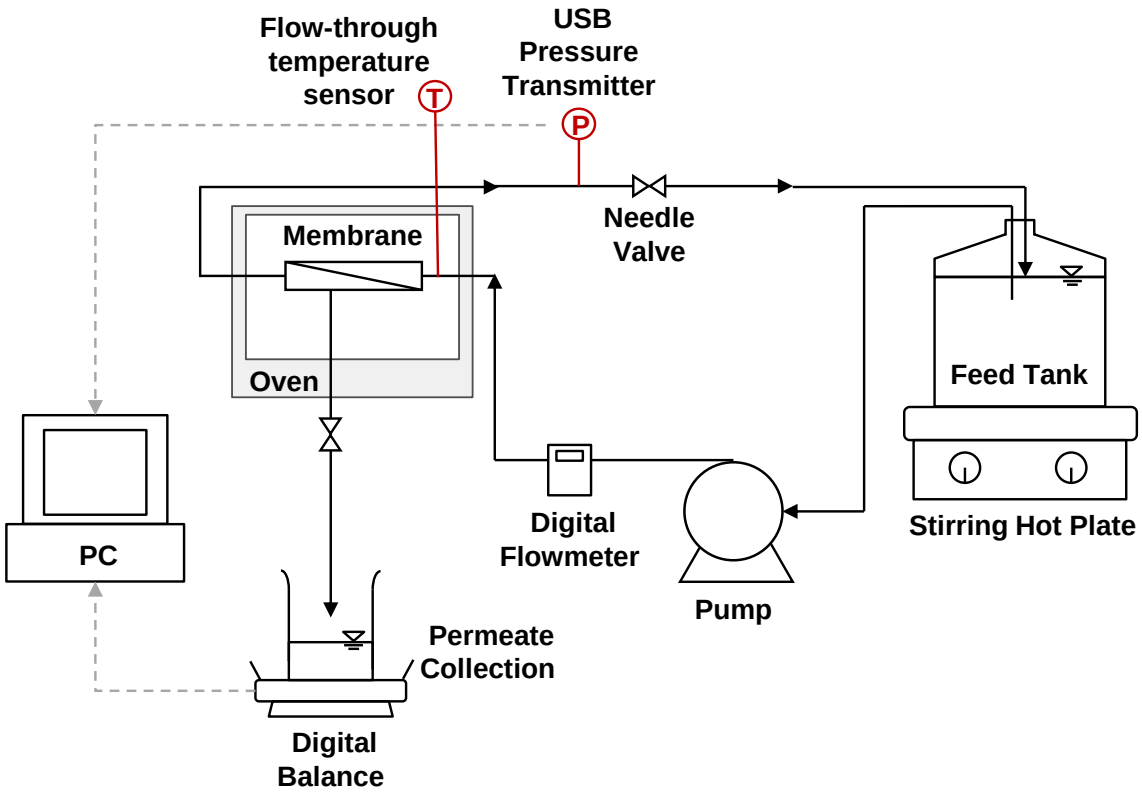

Fig. 1. Schematic diagram of the experimental setup. The membrane module is kept inside a temperature-controlled gravity convection oven and the permeate, collected on a digital balance, was returned frequently to the feed tank to simulate a total recycle mode.

Fig. 2. Photograph of experimental setup. The stainless steel membrane module can be seen in the bottom right, a spacer with a spiral channel created the tangential flow of solution across the surface of the membrane.

2.3. Resistance-in-series model analysis

Resistance-in-series model analysis was conducted using the terminal flux of the feed and pure water flux at different stages of cleaning. The pure water flux was calculated at the following three stages: before filtration with the clean membrane; after physical cleaning which included rinsing with ultrapure water, scrubbing with a soft sponge, and backwashing; and after

chemical cleaning. The terminal feed flux was the flux observed at the conclusion of the filtration of the feed solution. The resistance-in-series model, denoted by Eq. (1), was used to describe the fouling process:

$$J = \frac{\Delta P}{\eta R_t} = \frac{\Delta P}{\eta (R_m + R_{pr} + R_{cr} + R_{if})} \quad (1)$$

where J is the permeate flux [m/s]; ΔP is the TMP [Pa]; η is the dynamic viscosity [Pa·s]; and R's represent the resistances [m^{-1}] (R_t is the total resistance; R_m is the membrane resistance; R_{pr} is the resistance removable by physical cleaning methods; R_{cr} is the resistance removable by chemical cleaning; and R_{if} is the chemically irreversible resistance). The sum of all resistance components is the total resistance and the fouling resistance can be defined as the total resistance less R_m.

2.4. Solute rejection measurements

Solute rejection measurements were taken at set intervals throughout all filtration experiments by obtaining samples of the permeate. At all intervals the rejection rate was 100%. This corresponds well with the average pore size of the membrane, 4 nm, as reported by the manufacturer, and the measured average particle diameter of the colloidal silica particles, 34 nm. Furthermore, it was expected that all particles remained on the surface of the membrane forming a cake layer, rather than in the pores, due to the size difference between the particles and the membrane pores [27].

III. Results and Discussion

3.1. Effect of temperature on permeate flux

Fig. 3. shows the effect of feed temperature on the permeate flux during the filtration of colloidal silica nanoparticles at temperatures between 25 °C and 90 °C, pH 7.0, TMP 1.0 bar, and a cross-flow velocity of 0.60 m/s. From the permeate flux over the course of the filtration at each of the measured temperatures, the temperature effect is clearly seen with permeate flux increasing as a function of temperature increase [7-9, 28, 29]. The initial flux values showed a significant increase over the range of temperatures studied, increasing by 124% (91.6 to 205.0 LMH or $L \cdot m^{2} \cdot h^{-1}$) as temperature increased from 25 to 90 °C. The steady-state flux, or the final flux, also increased significantly, by 90% over the same range. The steady-state flux is defined as flux change less than 3.4% for at least 10 min. However, the effect was not as pronounced as it was for the initial values. Even though the increase in steady-state flux is not pronounced between 50 and 60 °C and 70 – 90 °C, the overall trend of increasing flux was noticeable. The approximate convergence of steady-state flux values between 70 and 90 °C is parallel to the findings of the study conducted by Lee et al. where steady-state flux converged between the temperatures of 10 – 30 °C [30]. This shows that the net effect of increasing temperature is higher steady-state flux values; however, small increases in temperature do not necessarily induce higher steady-state flux.

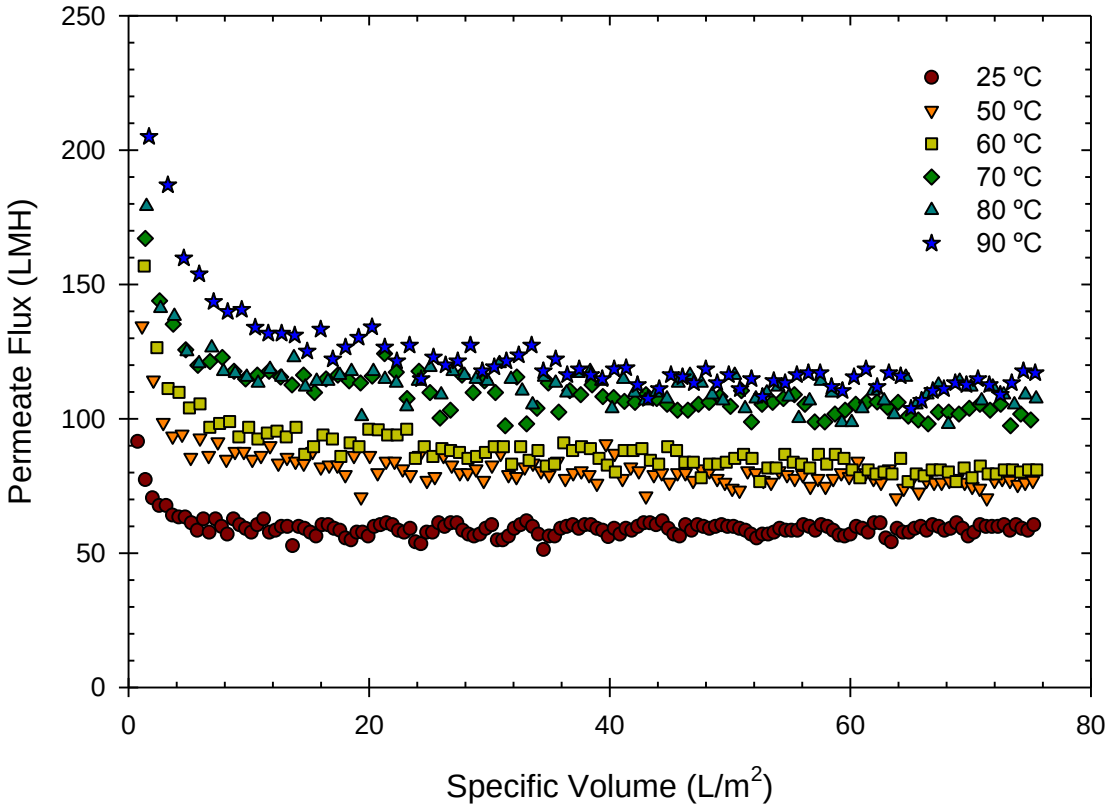

Fig. 3. The effect of feed temperature on the filtration of colloidal silica nanoparticles. The filtration runs were at 1.25 wt. % of colloidal silica, pH 7.0, cross-flow velocity of 0.60 m/s, and 1.0 bar.

The effect of temperature on pure water and feed permeate flux can be seen in Fig. 4. To further understand the contribution of the solution properties on the flux increase, the pure water flux was measured at temperatures between 25 °C and 90 °C with the same filtration conditions, but in the absence of colloidal silica. The viscosity of the feed solution containing the colloidal silica nanoparticles can be estimated from that of pure water as the concentration was very low at 1.25 wt. % and the pure water flux could serve as a comparison [31]. Initial feed and final, or steady-state, feed flux measurements were presented in order to see the change in fouling

potential and the effect on flux. The pure water, initial feed flux, and final feed flux were linear, i.e. R^2 values no less than 0.94, as indicated by the respective linear regressions. The initial permeate flux for the feed was less than the pure water flux in all experiments due to rapid initial fouling which resulted in a nearly instantaneous decrease in permeate flux. The difference in flux between pure water and initial feed flux increased with temperature, ranging from 22% (at 25 °C) to 48% (at 90 °C). The slope of the linear regression for the pure water flux was 4.1 LMH/°C while the slopes of the linear regressions for both the initial and final feed flux were 1.7 and 0.90 LMH/°C, respectively (Fig. 3). The slope of the pure water flux was 2.5 times larger and 4.6 times larger than the slopes of the initial and final feed flux. This indicated that the benefit to permeate flux from the increase in temperature and the subsequent decrease in viscosity diminished during filtration of the colloidal silica. In addition, it was evident that as filtration progressed, the temperature effect on the flux became less pronounced. The slope of the initial feed flux was 1.9 times larger than the slope of the final feed flux.

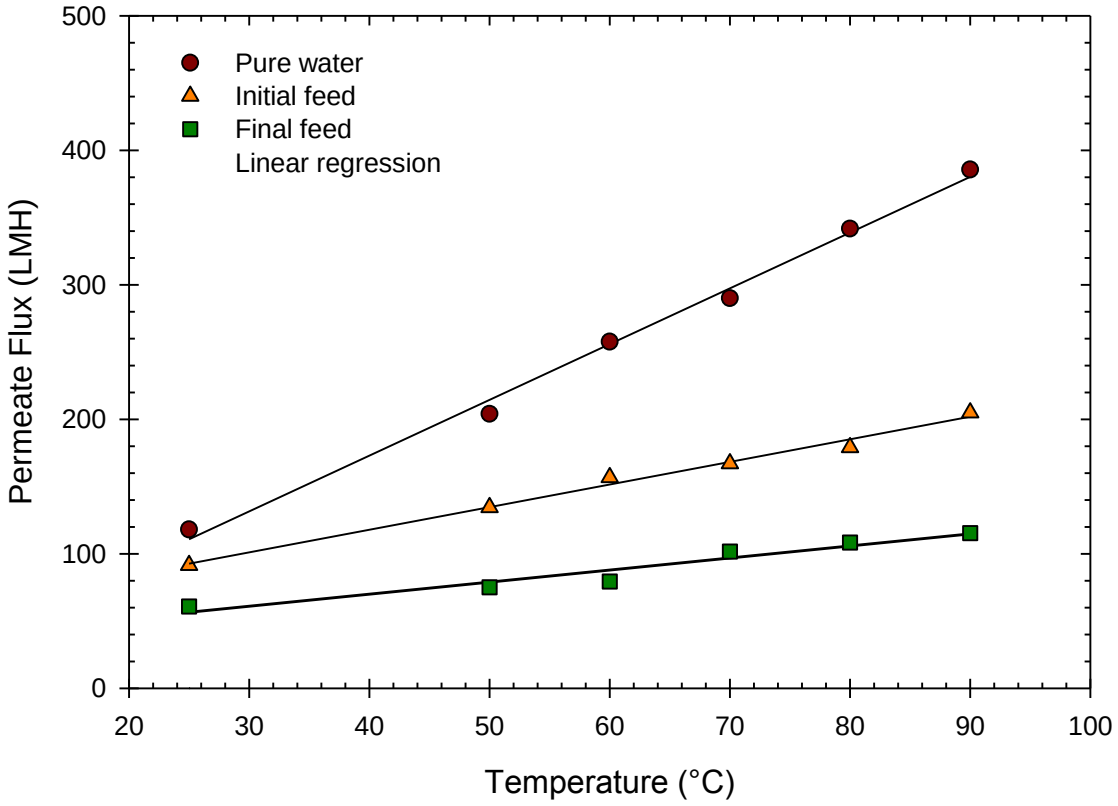

Fig. 4. A comparison of the effect of feed temperature on pure water and feed permeate flux. The results of linear were: $y = 4.1x + 7.2$ (R^2 = 0.99) for pure water (circle); $y = 1.7x + 51$ (R^2 = 0.99) for initial feed flux (triangle); and $y = 0.90x + 34$ (R^2 = 0.94) for final feed flux (square).

As the benefits of increasing temperature for flux in the filtration of the feed solution were not as clearly observed as expected from the viscosity change due to the elevated temperature, there is likely a factor negating the benefit. It is believed that the factor is related to the changes in the fouling potential as demonstrated in previous studies, using a membrane bioreactor and polymeric membranes for the treatment of wastewaters, which concluded that decreased permeate flux is not solely related to the viscosity, but also dependent on changes in

total resistance [32, 33]. The temperature dependency of pure water flux is directly related to the temperature dependency of viscosity, while the temperature dependency of water containing silica is not due to the diminished benefit of the temperature effect from fouling.

3.2. Resistance-in-series model analysis

Further insights on the result of the flux experiments were provided by the resistance-in-series model analysis shown in Fig. 5. The effect of temperature on the intrinsic membrane resistance was negligible as observed in previous studies [9, 30, 34, 35]. Total fouling resistance, or the total resistance less the intrinsic membrane resistance (R_t - R_m), was measured and was found to increase as temperature increased with a relationship of 5.8×10^{10} m^{-1}/°C. The predominant fouling resistance was the physically removable fouling, R_{pr} [30, 32, 36]. Total fouling resistance increased by 142% from 3.0×10^{12} m^{-1} (25 °C) to 7.3×10^{12} m^{-1} (90 °C), and R_{pr} increased by 280% from 2.5×10^{12} m^{-1} to 7.2×10^{12} m^{-1} over the same temperature range. On average, R_{pr} contributed 95% of the total fouling resistance. This provides confirmation that the dominant method of fouling in the filtration of colloidal silica solution was cake layer formation [37, 38]. Linear regression of R_{pr} revealed the slope to be 6.0×10^{10} m^{-1}/°C with an R^2 of 0.86, indicating that the increase in physically removable resistance was approximately linear.

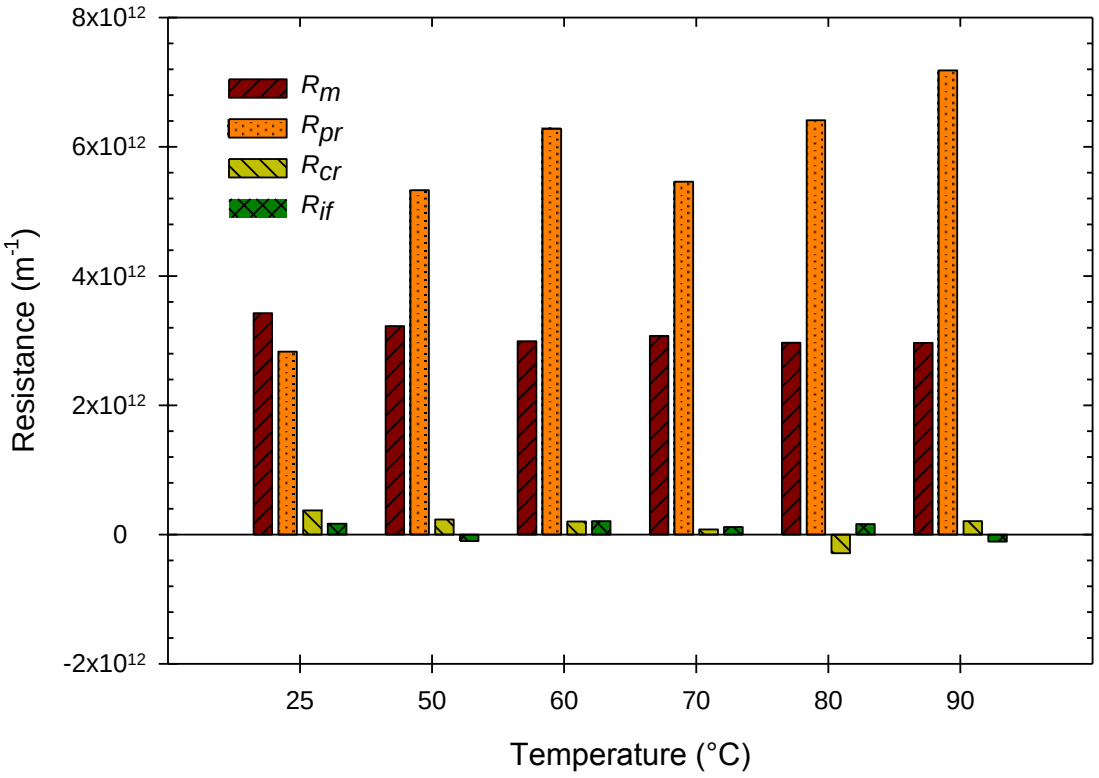

Fig. 5. Resistance-in-series model analysis of the temperature effect on filtration of colloidal silica. Eq. (1) was used to calculate the resistances. Linear regression of R_{pr} gives the equation: $y = 6.0\times10^{10}x + 1.8\times10^{12}$ with R^2 = 0.86.

Although the total fouling resistance increased as temperature increased, the greater amount of fouling was easily removed by simple physical cleaning procedures with nearly 100% of the initial flux recovery observed. The chemically removable and irreversible fouling were negligible at all temperatures, demonstrating that physical cleaning was very effective for the flux recovery of the ceramic membrane to a pristine state.

3.3. Effect of temperature on cake layer properties

The mass of particles deposited on the surface of the membrane during fouling was determined by collecting a sample of the initial and final feed solution [39]. Absorbance of the samples was measured with a UV-Vis spectrophotometer in order to determine the concentration. Assuming deposition of particles elsewhere in the system was negligible, the cake mass was then calculated using a mass balance, i.e. accumulation = mass in – mass out.

From the permeate flux and cake layer mass data, the cake porosity and thickness were calculated according to the methods adopted in a study by Faibish et al. [39]. Since R_{cr} and R_{if} were shown to be negligible, Eq. (1) can be rewritten as Eq. (2) with R_{m} and R_{pr} as the only contributing resistances:

$$J = \frac{\Delta P}{\eta\left(R_m + R_{pr}\right)} \tag{2}$$

where R_{pr} is the cake resistance. The specific cake resistance, α, can be calculated from R_{pr} using the following equation [40]:

$$R_{pr} = \alpha M_d \tag{3}$$

where M_d is the deposited mass per unit area on the membrane surface [g/m]. An important property of the cake layer is the cake porosity. Cake porosity is indicative of the tightness of the packing of particles in the cake, with a less porous cake layer having tighter packing which

restricts permeate flux. Cake porosity, ε, can be determined by the Carman-Kozeny equation [41]:

$$\alpha = \frac{45(1-\varepsilon)}{\rho a_p^2 \varepsilon^3} \tag{4}$$

where ρ is the particle density [kg/m^3] and a_p is the particle radius [m]. Thickness of the cake layer is also important in that a thicker cake layer will impede permeate flux. The cake layer thickness, δ_c, can be calculated using the cake layer mass data and a mass balance of the cake layer [42]:

$$\delta_c = \left(\frac{\frac{4}{3}\pi a_p^3}{1-\varepsilon} \right) M_c \tag{5}$$

where M_c is the number of particles accumulated in the cake layer per unit area. The cake layer mass, porosity, and thickness calculations allow for characterization of the cake and analysis of how these properties change with temperature.

Properties of the cake layer are shown in Fig. 6. The mass of the cake layer linearly increased as a function of temperature (Fig. 6(a)), and the primary source of permeate flux decline in this study was the deposition of particles on the surface of the membrane forming a cake layer. These results concur with the resistance-in-series model analysis results which showed that as temperature increased the physically removable fouling also increased linearly.

Greater particle deposition at higher temperatures causes an increase in resistance due to the increase in cake layer mass, which inhibits the permeate flux.

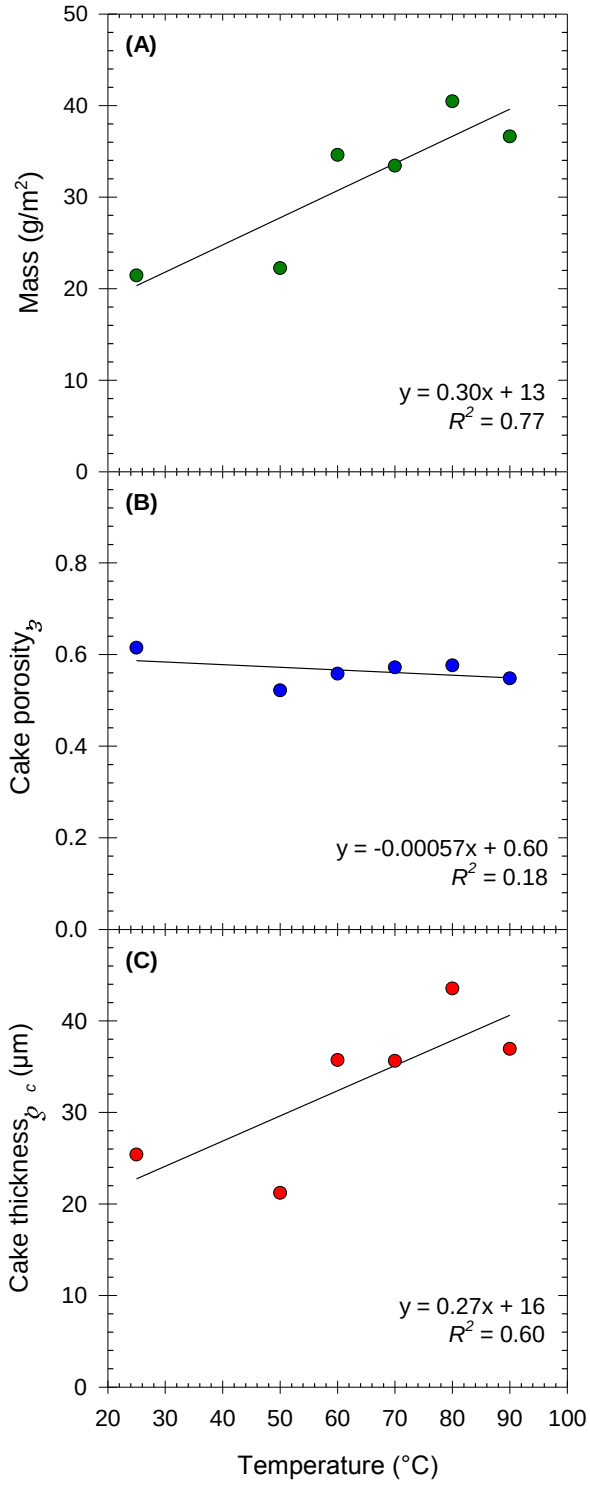

Fig. 6. Properties of the cake layer formed during the filtration of colloidal silica nanoparticles. (A) Mass of deposited particles per unit area of the membrane surface, (B) cake porosity, and (C) thickness of the cake layer.

The cake porosity and thickness are shown in Fig. 6(b) and Fig. 6(c), respectively. The cake porosity was independent of temperature, remaining at or slightly below 0.6 throughout the experiments. The linear increases in both cake thickness and the mass deposited data were in good agreement; each plot had a slope of approximately 0.3. As temperature increased, the cake thickness also tended to increase. Cake porosity is the volume fraction of voids in the cake layer divided by the total cake volume and can be viewed as a measurement of cake density. Since the cake porosity remained relatively unchanged as temperature increased, this indicated that the cake layer density was also constant. Hence, the increased cake layer mass due to elevated temperature directly related to the increase in the thickness of the cake layer. The measurement at 50 °C, with a slight increase in the cake mass but with relatively large decrease in the thickness of the cake, seemed to be caused by the porosity value at the temperature. The cake porosity at 50 °C was the smallest, and this resulted in the change in those parameters as expected from Eqs. (4) and (5); the cake layer was denser and the mass increased without a subsequent increase in the cake thickness. The results show that at elevated temperatures the cake layer properties changed in such a way that greater fouling of the membrane occurred.

3.4. Particle force balance

In order to gain further understanding of the increase in fouling with temperature, force balance analyses were conducted. There are several different forces acting on a particle during filtration, and these can be analyzed and summed into resultant forces. Fig. 7 shows the forces acting on a spherical particle during cross-flow filtration.

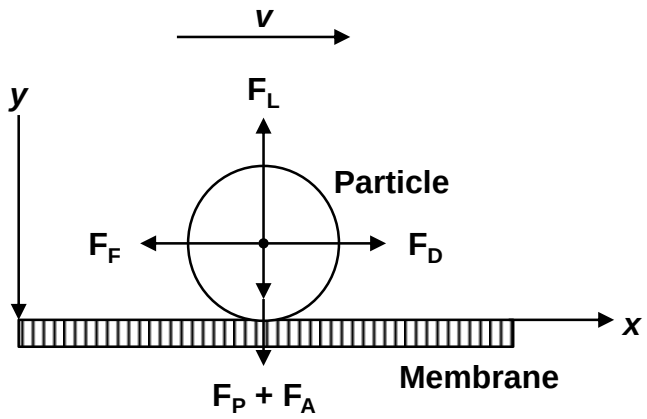

Fig. 7. Forces acting on a spherical particle in cross-flow filtration at the membrane surface. *x* is defined positive to the right as the direction of cross-flow, and *y* positive toward the membrane surface.

F_D and F_P are the drag forces associated with the cross-flow velocity and the permeate flux, respectively, F_L is the lift force caused by the shear flow, F_F is the friction force in opposition to the cross-flow velocity, and F_A is the adhesive force due to van der Waals and electrostatic interactions [43]. The drag forces, F_D and F_P, can be estimated using the Stoke's equation:

$$F_p = 3\pi\eta d_p J \tag{6}$$

where d_p is the particle diameter [m]. F_D is assumed to be 2.11 times the force calculated by the Stoke's equation, according to theoretical and experimental investigations [43], therefore, the equation for F_D is:

$$F_D = 2.11 \times 3\pi\eta d_p v_{\left(z=\frac{d_p}{2}\right)} \quad (7)$$

where $v_{(z\ =\ dp/2)}$ is the undistributed velocity at the position $z = d_p/2$ [44]. The undistributed velocity can be written as:

$$v_{\left(z=\frac{d_p}{2}\right)} = \frac{\tau_w d_p}{2\eta} \quad (8)$$

where τ_w is the shear stress [Pa]. Substituting Eq. (8) into Eq. (7) gives the following solution for F_D:

$$F_D = 3.16\pi\tau_w d_p^2 \quad (9)$$

Eqs. (6) and (9) are intended to be used for very low particle concentrations with no particle interaction, therefore, a correction factor, λ, must be applied [43]. For monodisperse particle solutions, the correction factor depends only on the volume concentration, φ_s [43]:

$$\lambda = \frac{4 + 3\varphi_s + 3\sqrt{8\varphi_s - 3\varphi_s^2}}{(2 - 3\varphi_s)^2} \quad (10)$$

The lift force, F_L, is the force directed away from the surface of the membrane and can be calculated from the following equation [43]:

$$F_L = 0.761 \frac{\tau_w^{1.5} d_p^3 \rho^{0.5}}{\eta} \quad (11)$$

The lift force and drag force of the permeate flow are primarily responsible for the deposition of particles in the cake layer. In the study by Altmann and Ripperger, it was shown that for small particle sizes the drag force is greater than the lift force and interpolation of their data down to particle sizes relevant to the current study indicate that this would likely be the case [43].

The van der Waals forces and electrostatic interactions are responsible for the adhesive force, F_A. By neglecting the electrostatic interactions, F_A can be estimated from the van der Waals force between two spheres[43]:

$$F_A = \frac{\hbar\varpi d_p}{32\pi a^2} \quad (12)$$

where $\hbar\varpi$ is the Lifschitz-van der Waals constant and a is the adhesive distance between two spheres, which were assumed to be 10^{-20} J and 0.4 nm, respectively [45]. The friction force, F_F, acts in opposition to the drag force of the cross-flow and is due to the normal force, F_N (adhesive force and drag force of the permeate flow). F_F is given by the following equation:

$$F_F = \mu F_N = \mu(F_A + F_P) \quad (13)$$

where μ is the coefficient of friction. The maximum value of μ (1.0) was assumed in all calculations [45].

The forces were summed according to the convention laid out in Fig. 7, and the resultant net forces were analyzed: F_x and F_y, in x- and y-directions, respectively. Note that x-direction is defined as the direction of cross-flow, and y-direction as the direction of permeation through the membrane. The effect of temperature on the resultant forces is shown in Fig. 8. As temperature increased, F_x decreased while F_y increased. The decrease in F_x indicates that as temperature increased the tangential force on particles in the solution was lessened. This decrease could have allowed more particles to settle and/or decreased the rate at which self-cleaning (removal of fouling from tangential flow) occurred. Subsequently, the vertical force toward the membrane surface, F_y, increased with temperature, which means greater force directed particles to the membrane surface. It is important to note that F_x is an order of magnitude larger than F_y. However, as was previously stated, the forces that make up F_y are primarily responsible for deposition, and therefore, the order of magnitude difference should not hinder cake formation. Linear regression was performed on both F_x and F_y, revealing linear correlations between the resultant forces and temperature with R^2 values no less than 0.93. The results of the force balance are in agreement with the filtration and fouling data where greater fouling resistance, cake layer mass, and cake thickness were observed at higher temperatures.

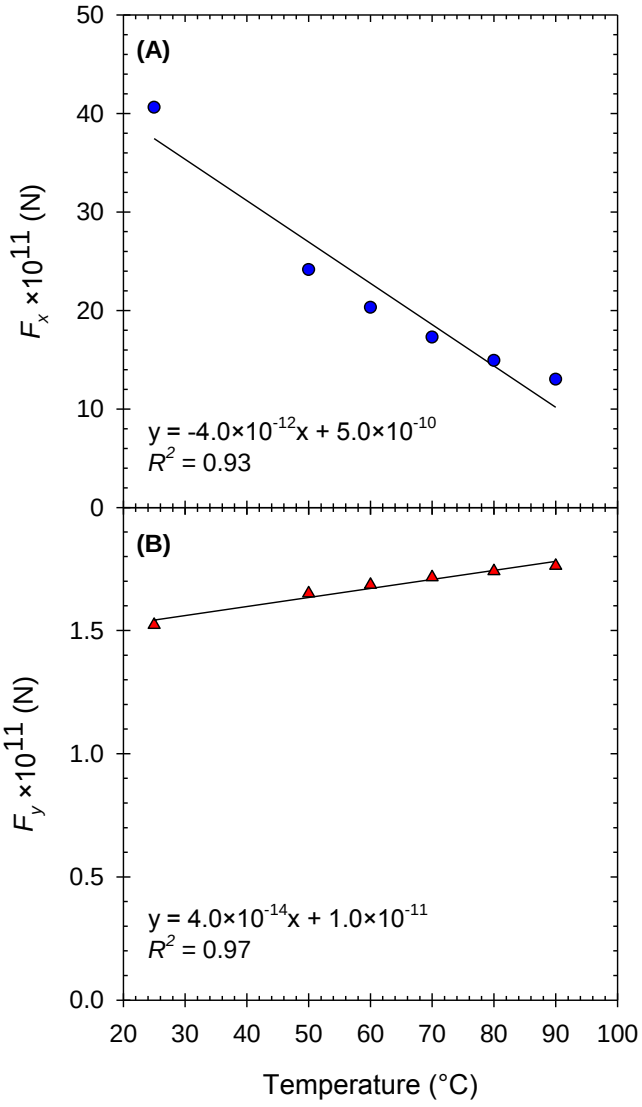

Fig. 8. Sum of the forces acting on a particle, in the *x*- (A) and *y*-directions (B), during cross-flow filtration of colloidal silica. The temperature effect is linear with R^2 values no less than 0.93.

IV. Conclusions and Future Studies

4.1. Conclusions

This study is one of the first of its kind to evaluate the effect of temperature on permeate flux decline and membrane fouling during the filtration of colloidal silica by ceramic ultrafiltration membranes. The benefits of increasing filtration temperature were clearly seen as the steady-state permeate flux nearly doubled with a temperature increase from 25 – 90 °C. Increasing permeate flux allows for a greater amount of feed solution to be treated in a shorter period of time which is an encouraging finding for application to industry. The benefit observed during filtration of the feed solution was less than that for filtration of pure water and this was attributed to the increased fouling resistance during feed filtration. A net positive effect on permeate flux was observed as flux increased with temperature in spite of the increased fouling. Fouling resistance increased primarily due to the increase in physically removable fouling or cake layer formation. These results are noteworthy because the increase in resistance is attributed to fouling that is easily removable by simple physical cleaning mechanisms such as rinsing, scrubbing, and/or backwashing. In most industrial water treatment facilities these are cleaning steps that are already performed periodically and the results of this study show that under certain operating conditions time consuming chemical cleaning processes could be alleviated or eliminated almost completely. The inherent properties of thermal and chemical resistance as well as mechanical robustness make ceramic membranes a potential filtration medium for these types of applications which should be explored further. The increased fouling resistance and cake layer mass and thickness with temperature can be explained using a force balance on a particle in the solution. As the temperature increased the tangential force decreased, meaning less self-cleaning

of the membrane surface occurred, while the vertical force increased causing greater particle deposition on the membrane surface.

4.2. Future Studies

Additional research is required to further study the mechanisms that provide the benefits of high temperature filtration and evaluate the applicability of this strategy in industrial processes. A pilot-scale study is imperative to see if the observed benefits are still evident when scaled up. An experimental determination of cake thickness and porosity using advanced microscopy is important to further characterize the cake layer and confirm the mathematically derived values in this study. Varying operational conditions and water quality parameters (i.e. temperature, cross-flow velocity, pressure, pH, feed concentration, ionic strength, organic foulants) to optimize the filtration process for different conditions is necessary for application to industry.

APPENDIX A. COLLOIDAL SILICA DATA

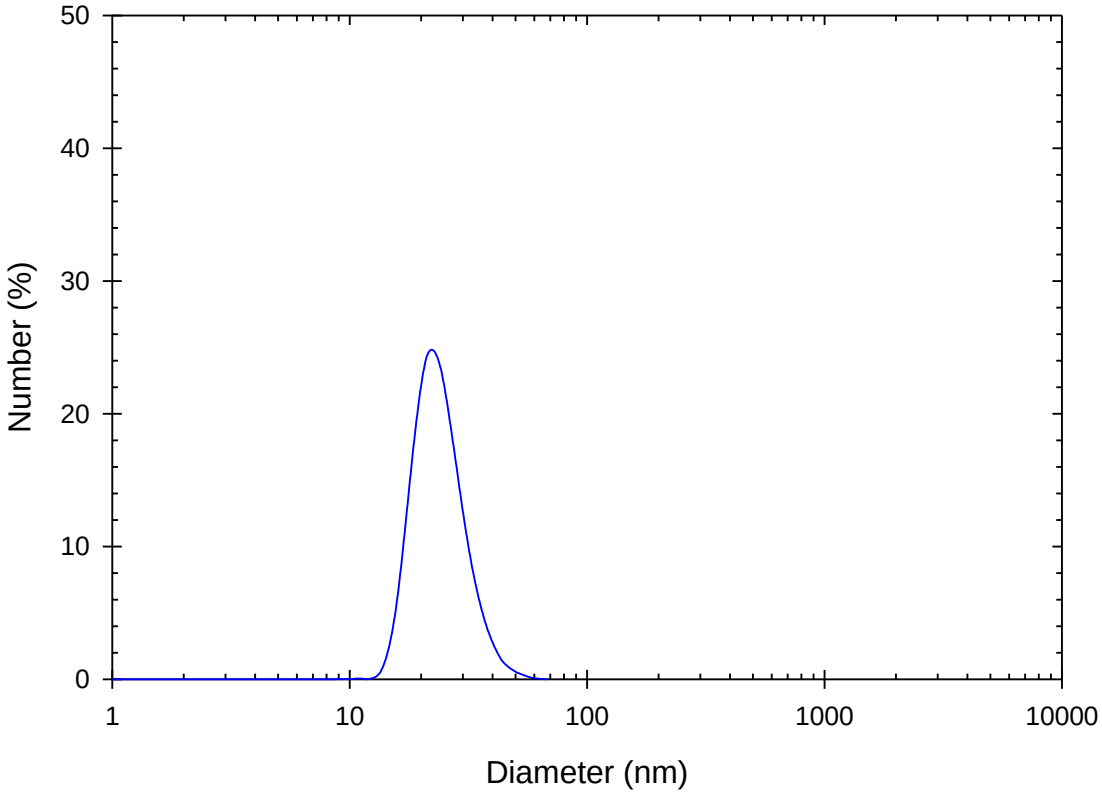

Fig. A1. Particle size distribution of LUDOX® AS-40 colloidal silica particles. The solution is monodisperse with an average particle diameter of 34 nm.

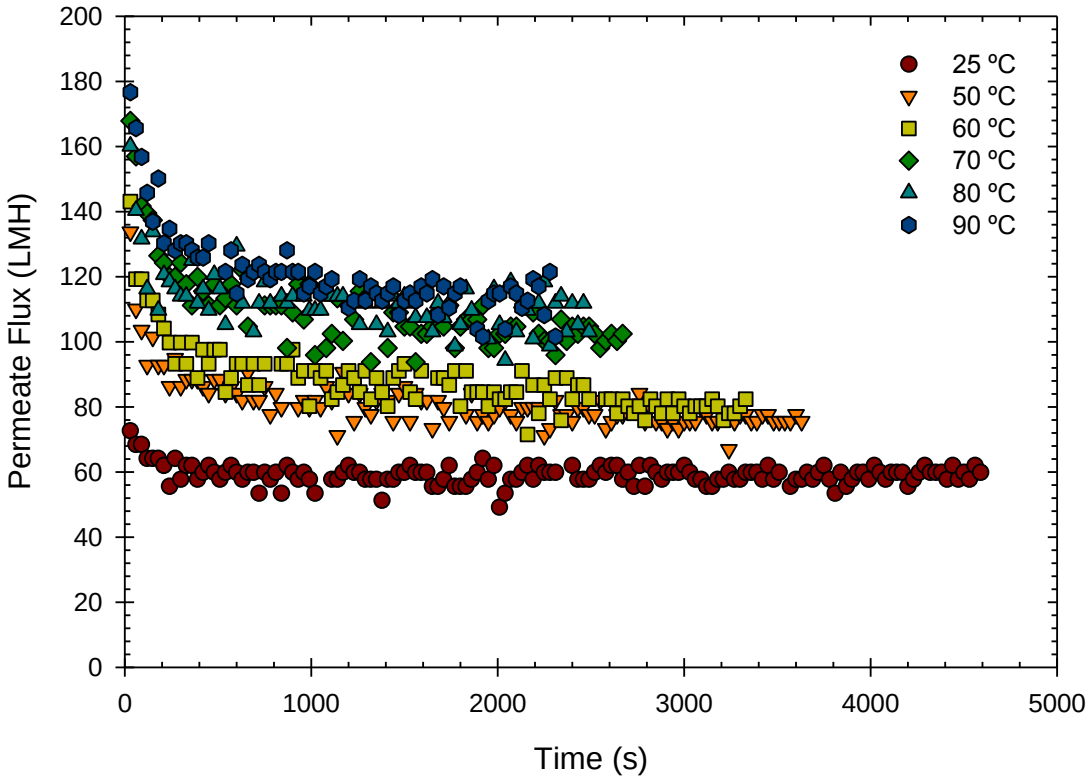

Fig. A2. The effect of feed temperature on the filtration of colloidal silica nanoparticles over time. The filtration runs were at 1.25 wt. % of colloidal silica, pH 7.0, cross-flow velocity of 0.60 m/s, and 1.0 bar.

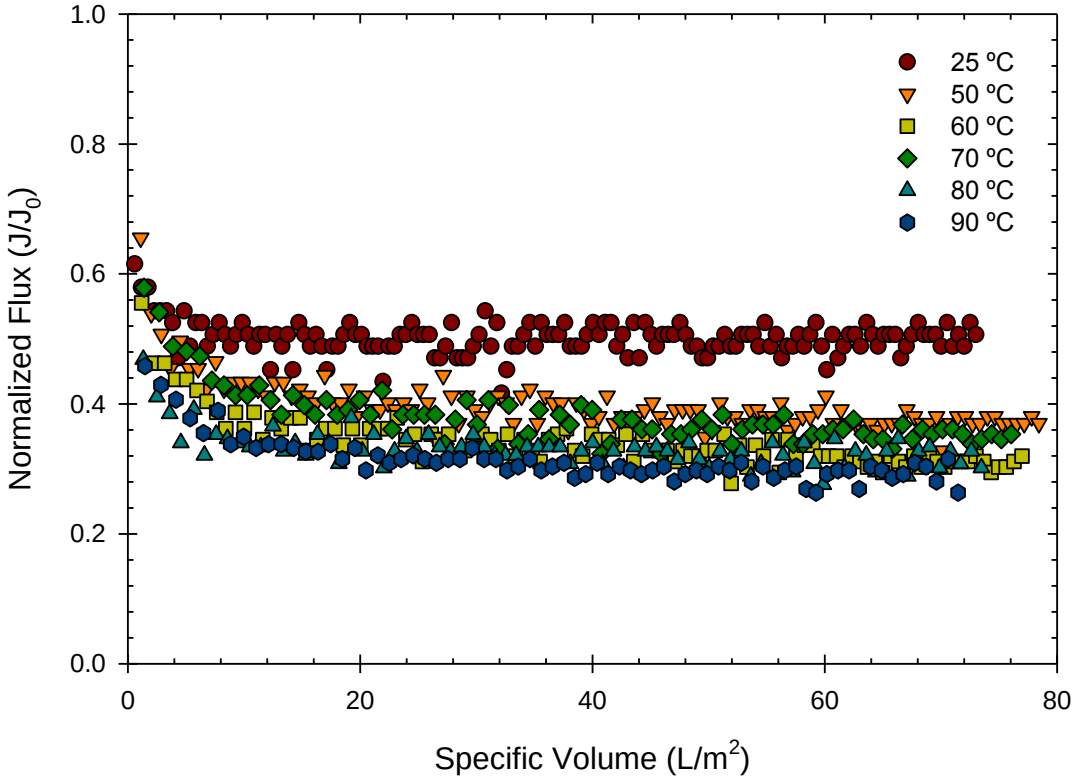

Fig. A3. The effect of feed temperature on normalized flux during the filtration of colloidal silica nanoparticles. Normalized flux is calculated by dividing the permeate flux (J) by the pure water flux (J_0). The filtration runs were at 1.25 wt. % of colloidal silica, pH 7.0, cross-flow velocity of 0.60 m/s, and 1.0 bar.

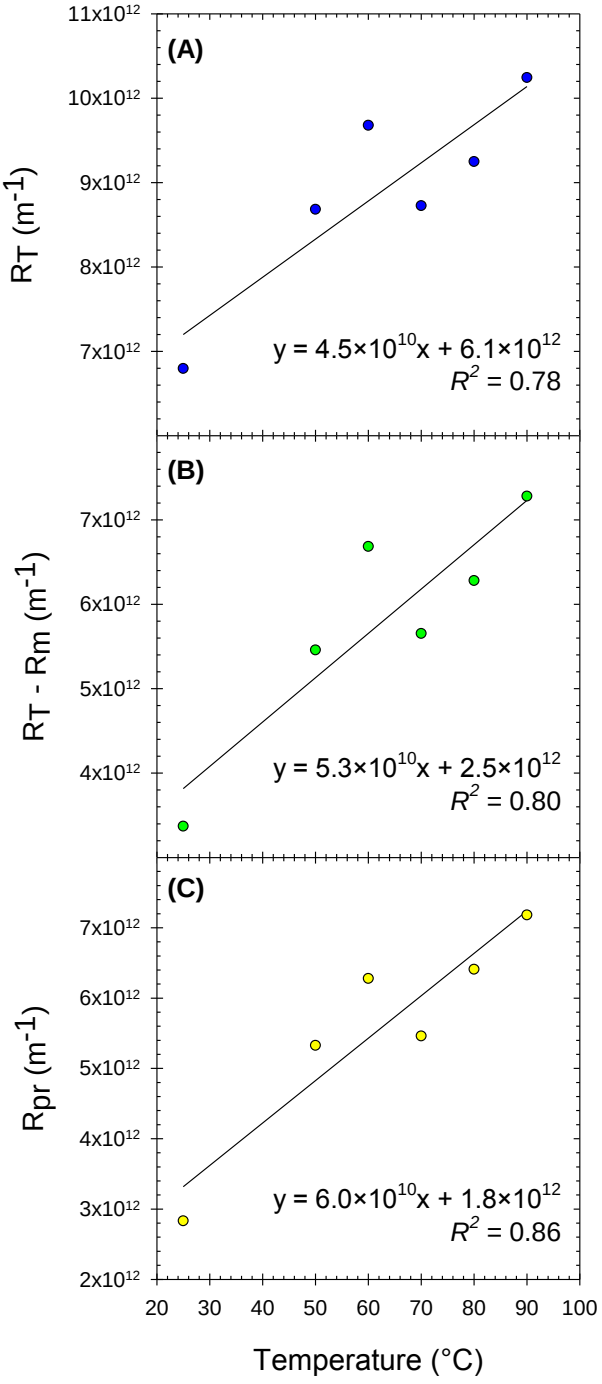

Fig. A4. The effect of feed temperature on (A) the total resistance (R_T), (B) fouling resistance (R_T-R_m), and (C) physically removable resistance (R_{pr}). Linear regression shows that the plots are essentially linear with R^2 values no less than 0.78

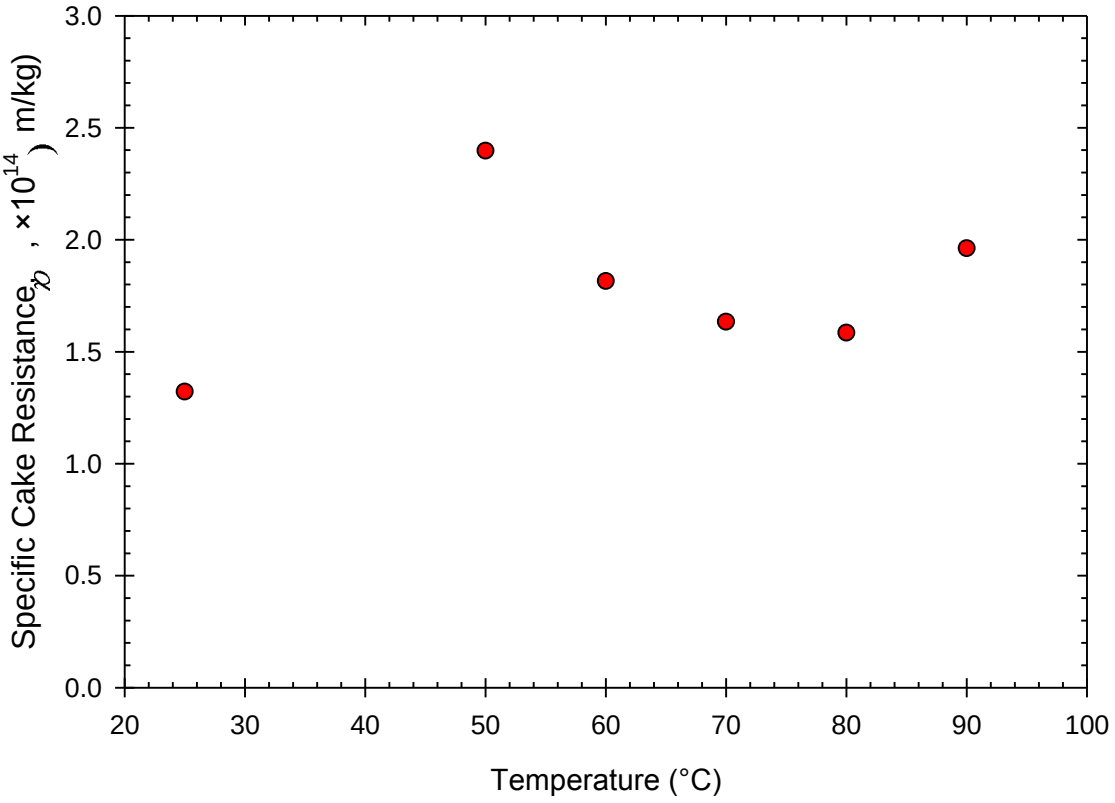

Fig. A5. The effect of feed temperature on specific cake resistance, *α*, calculated from Eq. (3). The filtration runs were at 1.25 wt. % of colloidal silica, pH 7.0, cross-flow velocity of 0.60 m/s, and 1.0 bar.

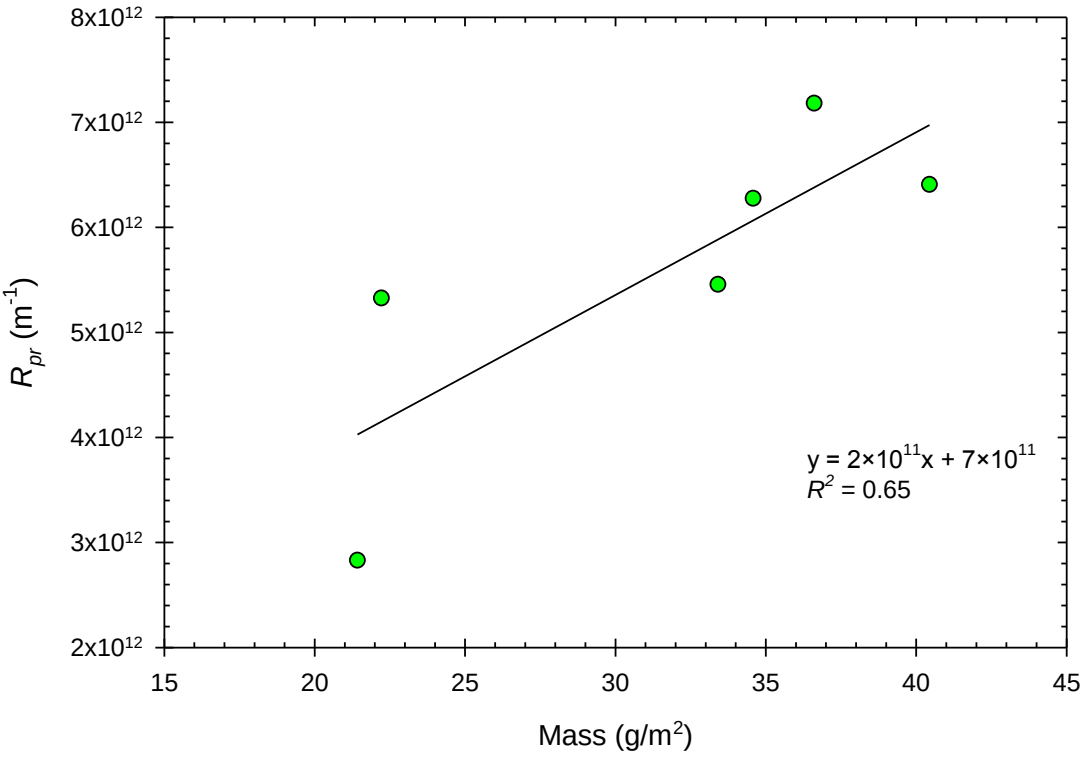

Fig. A6. Physically removable resistance, R_{pr}, versus the mass deposited, M_d, during filtration at feed temperatures between 25 – 90 °C. The filtration runs were at 1.25 wt. % of colloidal silica, pH 7.0, cross-flow velocity of 0.60 m/s, and 1.0 bar. Linear regression was used to plot the trend and the R^2 value was 0.65, indicating a fairly linear correlation.

APPENDIX B. SYNTHETIC FGD WASTEWATER DATA

Table B1. Composition of the synthetic FGD wastewater and the source chemicals used to create it. Feed solutions were made by mixing the source chemicals into 2L of pure water and adding acid or base to achieve a pH of 7.0.

Source	Concentration (mg/L)	Constituents	Concentration (mg/L)
NaCl	2000	Cl^-	11000
$CaCl_2$ (anhydrous)	5500	SO_4^{2-}	2500
Na_2SO_4 (anhydrous)	3700	Ca^{2+}	2000
$MgCl_2$ (hexahydrate)	17000	Mg^{2+}	2000
SiO_2	5000	Na^+	2000
		SiO_2	5000

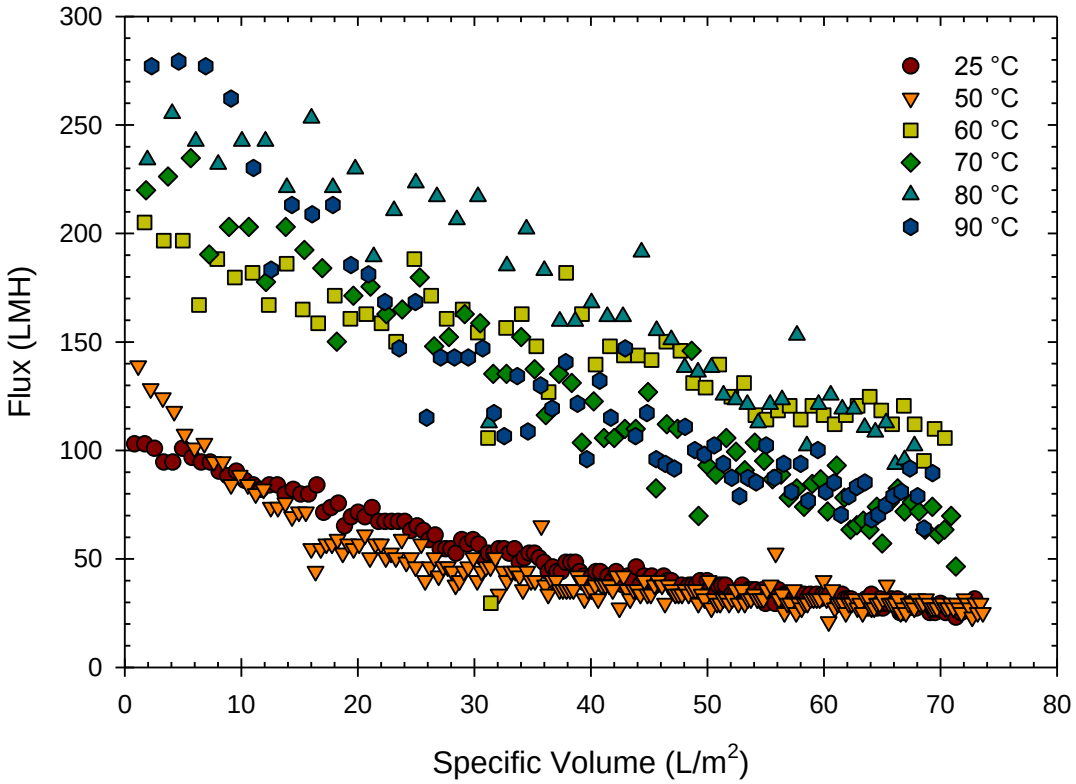

Fig. B1. The effect of feed temperature on the filtration of synthetic FGD wastewater over the temperature range 25 – 90 °C using a 50 kDa ceramic membrane. Experimental conditions were: pH 7.0, cross-flow velocity of 0.60 m/s, and pressure 1.0 bar.

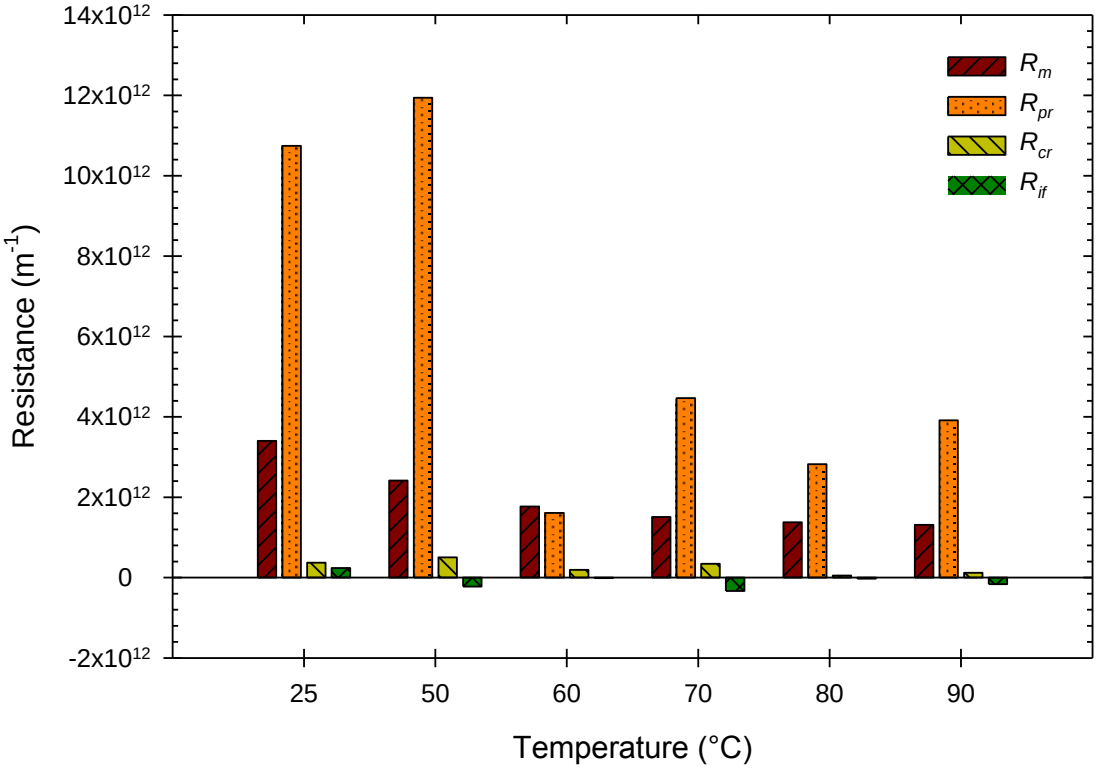

Fig. B2. Resistance-in-series model analysis of the temperature effect on filtration of synthetic FGD wastewater. Eq. (1) was used to calculate the resistances.

REFERENCES

[1] M. Mänttäri, A. Pihlajamäki, E. Kaipainen, M. Nyström, Effect of temperature and membrane pre-treatment by pressure on the filtration properties of nanofiltration membranes, Desalination, 145 (2002) 81-86.

[2] X. Qu, W.J. Gao, M.N. Han, A. Chen, B.Q. Liao, Integrated thermophilic submerged aerobic membrane bioreactor and electrochemical oxidation for pulp and paper effluent treatment – towards system closure, Bioresource Technology, 116 (2012) 1-8.

[3] G. Daufin, J.P. Escudier, H. Carrère, S. Bérot, L. Fillaudeau, M. Decloux, Recent and Emerging Applications of Membrane Processes in the Food and Dairy Industry, Food and Bioproducts Processing, 79 (2001) 89-102.

[4] J. Sójka-Ledakowicz, T. Koprowski, W. Machnowski, H.H. Knudsen, Membrane filtration of textile dyehouse wastewater for technological water reuse, Desalination, 119 (1998) 1-9.

[5] C. Allègre, P. Moulin, M. Maisseu, F. Charbit, Treatment and reuse of reactive dyeing effluents, J. Membr. Sci., 269 (2006) 15-34.

[6] T. Higgins, A. Sandy, S. Givens, Flue Gas Desulfurization Wastewater Treatment Primer, Power, 153 (2009).

[7] M. Cheryan, Ultrafiltration handbook, Lancaster, Pa. : Technomic Pub. Co., c1986., 1986.

[8] M. Kallioinen, M. Manttari, M. Nystrom, J. Nuortila-Jokinen, Effect of high filtration temperature on regenerated cellulose ultrafiltration membranes, Separation Science and Technology, 42 (2007) 2863-2879.

[9] G.T. Vladisavljevic, S.K. Milonjic, D. Nikolic, V.L. Pavasovic, Influence of temperature on the ultrafiltration of silica sol in a stirred cell, J. Membr. Sci., 66 (1992) 9-17.

[10] S. Freeman, H. Shorney-Darby, What's the Buzz About Ceramic Membranes?, American Water Works Association. Journal, 103 (2011) 12-13.

[11] M. Cheryan, Ultrafiltration and Microfiltration Handbook, Taylor & Francis, 1998.

[12] M.J.H. Snow, D. de Winter, R. Buckingham, J. Campbell, J. Wagner, New techniques for extreme conditions: high temperature reverse osmosis and nanofiltration, Desalination, 105 (1996) 57-61.

[13] K. Krynicki, C.D. Green, D.W. Sawyer, Pressure and temperature dependence of self-diffusion in water, Faraday Discussions of the Chemical Society, 66 (1978) 199-208.

[14] M.-C. Vincent-Vela, B. Cuartas-Uribe, S. Álvarez-Blanco, J. Lora-García, Analysis of an ultrafiltration model: Influence of operational conditions, Desalination, 284 (2012) 14-21.

[15] S. Garcia-Garcia, M. Jonsson, S. Wold, Temperature effect on the stability of bentonite colloids in water, Journal of colloid and interface science, 298 (2006) 694-705.

[16] X. Zhu, M. Elimelech, Colloidal fouling of reverse osmosis membranes: measurements and fouling mechanisms, Environmental Science & Technology, 31 (1997) 3654-3662.

[17] S.-J. Lee, M. Dilaver, P.-K. Park, J.-H. Kim, Comparative analysis of fouling characteristics of ceramic and polymeric microfiltration membranes using filtration models, J. Membr. Sci., 432 (2013) 97-105.

[18] M.O. Lamminen, H.W. Walker, L.K. Weavers, Mechanisms and factors influencing the ultrasonic cleaning of particle-fouled ceramic membranes, J. Membr. Sci., 237 (2004) 213-223.

[19] S.-H. Lee, K.-C. Chung, M.-C. Shin, J.-I. Dong, H.-S. Lee, K.H. Auh, Preparation of ceramic membrane and application to the crossflow microfiltration of soluble waste oil, Materials Letters, 52 (2002) 266-271.

[20] J. Finley, Ceramic membranes: a robust filtration alternative, Filtration & Separation, 42 (2005) 34-37.

[21] K. Guerra, J. Pellegrino, Development of a Techno-Economic Model to Compare Ceramic and Polymeric Membranes, Separation Science and Technology, 48 (2012) 51-65.

[22] I.H. Huisman, D. Elzo, E. Middelink, A.C. Trägårdh, Properties of the cake layer formed during crossflow microfiltration, Colloids and Surfaces A: Physicochemical and Engineering Aspects, 138 (1998) 265-281.

[23] G. Singh, L. Song, Experimental correlations of pH and ionic strength effects on the colloidal fouling potential of silica nanoparticles in crossflow ultrafiltration, J. Membr. Sci., 303 (2007) 112-118.

[24] G. Singh, L. Song, Impact of feed water acidification with weak and strong acids on colloidal silica fouling in ultrafiltration membrane processes, Water Res, 42 (2008) 707-713.

[25] A.B. Koltuniewicz, R.W. Field, T.C. Arnot, Cross-flow and dead-end microfiltration of oily-water emulsion. Part I: Experimental study and analysis of flux decline, J. Membr. Sci., 102 (1995) 193-207.

[26] T. Nakajima, K. Yamada, H. Idehara, H. Takanashi, A. Ohki, Removal of Selenium (VI) from Simulated Wet Flue Gas Desulfurization Wastewater Using Photocatalytic Reduction, Journal of Water and Environment Technology, 9 (2011) 13-19.

[27] E.S. Tarleton, R.J. Wakeman, Understanding flux decline in crossflow microfiltration: Part I - Effects of particle and pore size, Chemical Engineering Research and Design, 71 (1993) 399-410.

[28] Y. Zhao, Y. Zhang, W. Xing, N. Xu, Treatment of titanium white waste acid using ceramic microfiltration membrane, Chemical Engineering Journal, 111 (2005) 31-38.

[29] J. Lindmark, E. Thorin, J. Kastensson, C.M. Pettersson, Membrane filtration of process water at elevated temperatures—A way to increase the capacity of a biogas plant, Desalination, 267 (2011) 160-169.

[30] H. Lee, S.G. Kim, J.S. Choi, S.K. Kim, H.J. Oh, W.T. Lee, Effects of water temperature on fouling and flux of ceramic membranes for wastewater reuse, Desalination and Water Treatment, 51 (2013) 5222-5230.

[31] P.C. Hiemenz, R. Rajagopalan, Principles of Colloid and Surface Chemistry, Third Edition, Revised and Expanded, Taylor & Francis, 1997.

[32] C. Chiemchaisri, K. Yamamoto, Performance of membrane separation bioreactor at various temperatures for domestic wastewater treatment, J. Membr. Sci., 87 (1994) 119-129.

[33] W. Shu-Sen, Effect of solution viscosity on ultrafiltration flux, J. Membr. Sci., 39 (1988) 187-194.

[34] I.H. Huisman, B. Dutré, K.M. Persson, G. Trägårdh, Water permeability in ultrafiltration and microfiltration: Viscous and electroviscous effects, Desalination, 113 (1997) 95-103.

[35] S.F. Boerlage, Scaling and Particulate Fouling in Membrane Filtration Systems, Taylor & Francis, 2001.

[36] Z. Beril Gönder, S. Arayici, H. Barlas, Advanced treatment of pulp and paper mill wastewater by nanofiltration process: Effects of operating conditions on membrane fouling, Separation and Purification Technology, 76 (2011) 292-302.

[37] M. Zhang, L. Song, Mechanisms and Parameters Affecting Flux Decline in Cross-Flow Microfiltration and Ultrafiltration of Colloids, Environmental Science & Technology, 34 (2000) 3767-3773.

[38] V. Lahoussine-Turcaud, M.R. Wiesner, J.-Y. Bottero, Fouling in tangential-flow ultrafiltration: The effect of colloid size and coagulation pretreatment, Journal of Membrane Science, 52 (1990) 173-190.

[39] R.S. Faibish, M. Elimelech, Y. Cohen, Effect of Interparticle Electrostatic Double Layer Interactions on Permeate Flux Decline in Crossflow Membrane Filtration of Colloidal Suspensions: An Experimental Investigation, Journal of colloid and interface science, 204 (1998) 77-86.

[40] A.A. McCarthy, P.K. Walsh, G. Foley, Experimental techniques for quantifying the cake mass, the cake and membrane resistances and the specific cake resistance during crossflow filtration of microbial suspensions, J. Membr. Sci., 201 (2002) 31-45.

[41] G. Belfort, R.H. Davis, A.L. Zydney, The behavior of suspensions and macromolecular solutions in crossflow microfiltration, J. Membr. Sci., 96 (1994) 1-58.

[42] S. Hong, R.S. Faibish, M. Elimelech, Kinetics of Permeate Flux Decline in Crossflow Membrane Filtration of Colloidal Suspensions, Journal of colloid and interface science, 196 (1997) 267-277.

[43] J. Altmann, S. Ripperger, Particle deposition and layer formation at the crossflow microfiltration, Journal of Membrane Science, 124 (1997) 119-128.

[44] H.K. Vyas, R.J. Bennett, A.D. Marshall, Cake resistance and force balance mechanism in the crossflow microfiltration of lactalbumin particles, Journal of Membrane Science, 192 (2001) 165-176.

[45] J. Visser, Particle adhesion and removal: A review, Particulate Science and Technology, 13 (1995) 169-196.